

# CO6-1 Measurement of Transmittance Spectra of a Cryo-Sectioned Tissue of Brain Tumor C6 Model in the Terahertz Region

N. Miyoshi and T. Takahashi<sup>1</sup>

Department of Tumor Pathology, Faculty of Medicine, University of Fukui, and

<sup>1</sup> Research Reactor Institute, Kyoto University

**INTRODUCTION:** The LINAC (linear particle accelerator) technology in the milli and tera-hertz waves had been unique and had been used as a coherent synchrotron light in the research reactor institute of Kyoto university (KURRI) to observe the transmittance spectra of a sectioned tissue of raw brain tumor C6 model as a collaborate study. The absorption spectra in the tera-hertz region had been not so clear for the raw tumor tissue although Ashworth-PC. et al. [1] had reported for the excised human breast cancer by a terahertz pulsed spectroscopy observed at 320 GHz, which was estimated a longer relaxation time component of the induced electricity for water molecules [2-3] in the raw tumor tissue.

We also estimated what kind of water molecules become dominant in the viable and necrotic cancer regions by the different measurement method as an aim of this study.

**EXPERIMENTS:** (1) Instrument of Near-field in tera-hertz region: The photograph of the instrument was shown in Fig. 1. Mark-A: Pre-probe Wiston cone; 50-10mm diameter, Length=60mm; the irradiate diame-ter=0.775mm; The concentrate light probe (diame-ter)=3mm. The instrument was developed by Dr. T. Takahashi in KURRI. [Fig. 1]



(2) Sample preparation: A cryo-sectioned (thickness=100 μm) tissue was prepared from the raw C6 glial tumor model using a Cryo-section Maker (Leica) and was sealed sandwich-type with saran-wrap film (thickness=10 μm) in Figures 2-3 or with 2 plates of cover glasses (thickness=130-170 μm) in Figure 4, respectively under freezing condition (-20 C) before the measurements.

**RESULTS:** Two different penetration materials of saran-wrap film and cover glasses were mapping measured of spectra of two different C6 tumor model tissues as shown in Figures 2-3 and Figure 4, respectively.

[Fig. 2] H.&E.-stained Images and linear mapping line and the transmitted spectra

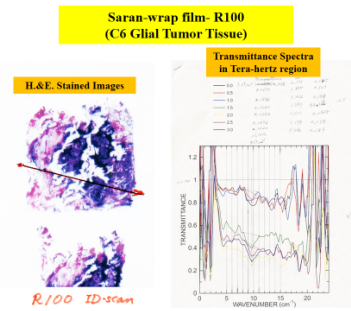


[Fig. 3] H.& E.-stained Images and linear mapping line and the absorbance at 9.69 cm<sup>-1</sup>

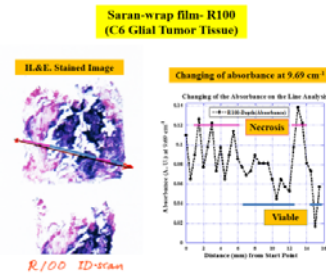
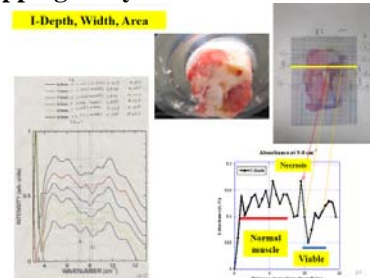


[Fig. 4] C6 glial tumor model tissue, the H.&E.-stained Image, the transmit spectra, and the linear mapping analysis of the different depth areas-I



From these 2 linear mapping data (Figures-3, and 4), there were presented higher absorbance components at 7-9 cm<sup>-1</sup> in necrotic cancer region in these linear analysis from Figures 3 and 4 even the penetrate materials were different. It was estimated that the specific water molecules at 7-9 cm<sup>-1</sup> region might be presented in the necrotic cancer area which the large amount of lipid components induced in the necrotic cancer area. These environment condition will control the water molecule conformation (looks like a free water which the hydrogen bond will be longer, 0.295 nm than that, 0.273 nm of the binding water molecules in viable cancer area) around the lipid components in the cancer region. These estimation will be more needed to be reappear the spectra, especially, the diffraction effect in these spectra data to remove from the data.

## REFERENCES:

- [1] P. C. Ashworth, *et al.*, Optics Express, **17(14)** (2009) 12444-12454.
- [2] T. Fukasawa, *et al.*, Phys. Rev. Let., **95** (2005) 197802.
- [3] Hiroyuki Yada, *et al.*, Chem. Phys. Let., **464** (2008) 166-170.

## Carotenoid-Producing *Lactobacillus plantarum* Is Resistant to $\gamma$ -Ray Irradiation

K. Oda, T. Saito<sup>1</sup>, Y. Matoba, Y. Kubono, M. Noda, T. Kumagai and M. Sugiyama

*Department of Molecular Microbiology and Biotechnology, Graduate School of Biomedical and Health Sciences, Hiroshima University*

<sup>1</sup>*Research Reactor Institute, Kyoto University*

**INTRODUCTION:** Carotenoids are a group of colored terpenoids with antioxidant properties. Especially, carotenoids have a unique radical scavenging and singlet oxygen quenching activities [1]. Therefore, carotenoids may prevent the organism from  $\gamma$ -ray irradiation through its scavenging and quenching activities. Lactic acid bacteria (LAB) are Gram-positive, low-GC, microaerophilic, rod or cocci that ferment sugar to produce lactic acid, and have been used to ferment foods for at least 4000 years. Carotenoid-producing LAB may have an industrially worth for producing the fermented food with antioxidant effect. *Lb. plantarum* is one of LAB species used as probiotic microorganism for many fermented foods. In this study, we investigated whether carotenoid-producing *Lb. plantarum* strains are resistant to  $\gamma$ -ray irradiation.

**EXPERIMENTS:** *Lb. plantarum* strains used in this study are described in Table 1. For their culturing, MRS broth (Merck) were used. Each strain was grown in MRS broth at 30°C for 24 h, and the resulting broth contained about  $2 \times 10^9$  cells per ml. Before irradiation, cells were washed with PBS buffer and resuspended into the same buffer. Cell suspensions were irradiated with  $\gamma$ -ray from a <sup>60</sup>Co source at a dose rate of 717 Gy per h. To measure the number of surviving bacteria after irradiation, irradiated cell cultures were diluted appropriately, and then plated on MRS agar in triplicate. Plates were incubated at 30°C and colonies were counted after 72 h of incubation. In Fig. 1, log of the ratio of the number after the treatment with irradiation to that without irradiation is plotted against the total dose.

**RESULTS AND DISCUSSION:** As shown in Fig. 1,  $\gamma$ -ray irradiation experiments indicated that  $D_{10}$  of two carotenoid-producing strains against the  $\gamma$ -ray irradiation (470 and 430 Gy for 3930 and SN35N strains, respectively) was higher than that of carotenoid-nonproducing strain (190 Gy for SN13T strain). In addition, SN13T is more sensitive toward the exposure of hydrogen peroxide, one of the active oxygen, than 3930 and SN35N (Table 1). These results suggested that carotenoid produced by LAB is involved in the protection from active oxygen generated by  $\gamma$ -ray irradiation and from hydrogen peroxide. On the other hand, whereas 3930 and SN35N show almost

the same resistance toward  $\gamma$ -ray irradiation, MIC toward hydrogen peroxide of 3930 (8 mM) was higher than that of SN35N (6 mM). SN35N produces a plenty of extracellular polysaccharide, but 3930 and SN13T do not. The extracellular polysaccharides produced may be involved in the resistance toward hydrogen peroxide in the SN35N strain.

Table 1.

*Lactobacillus plantarum* strains

Strain	Carotenoid production <sup>a</sup>	Extracellular polysaccharide production <sup>b</sup>	MIC toward H <sub>2</sub> O <sub>2</sub> <sup>c</sup> (mM)
3930	+	-	8
SN35N	+	+	6
SN13T	-	-	4

<sup>a</sup> Judged by color of the cell pellets obtained after centrifugation: +, yellow; -, white.

<sup>b</sup> Judged by turbidity of culture supernatant after centrifugation: +, cloudy; -, clear.

<sup>c</sup> Hydrogen peroxide resistance assay were carried using overnight cultures grown at 30°C. Cells were washed with PBS buffer and resuspended into the same buffer.  $1 \times 10^4$  cells per spot was loaded on MRS agar containing indicated concentration (4, 6, and 8 mM) of hydrogen peroxide, which was prepared at the time of use. Plates were incubated at 30°C for 72 h. MIC, minimum inhibitory concentration.

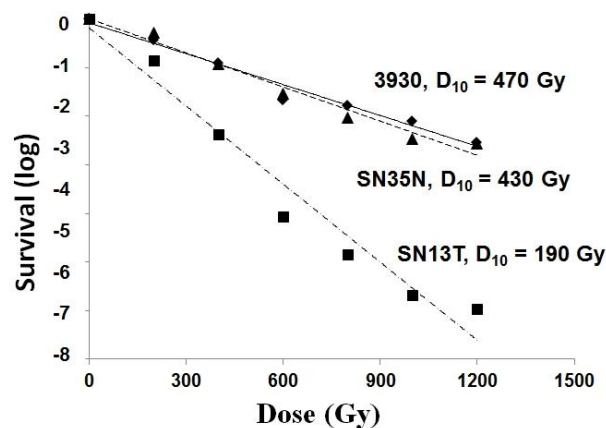


Fig. 1. Response of *Lb. plantarum* strains to  $\gamma$ -ray irradiation. Strains were irradiated with the indicated dose of  $\gamma$ -ray and the survival ratio was measured as described above.  $\blacklozenge$ , 3930;  $\blacktriangle$ , SN35N;  $\blacksquare$ , SN13T.  $D_{10}$  represents the dose of irradiation causing death for 90 % of total cells.

### REFERENCES:

- [1] A. Clauditz *et al.*, *Infect Immun.*, **74** (2006) 4950-4953.

K. Akamatsu, N. Shikazono and T. Saito<sup>1</sup>

*Irradiated Cell Analysis Research Group, Quantum Beam Science Directorate, Japan Atomic Energy Agency*

<sup>1</sup>*Research Reactor Institute, Kyoto University*

**INTRODUCTION:** It is known that DNA lesions induced by ionizing radiation and chemicals can cause mutation and carcinogenesis. In particular, ‘clustered damage’ site, that is a DNA region with multiple lesions within one or two helical turns, is believed to be hardly repaired. This damage is considered to be induced, e.g., around high-LET ionizing radiation tracks. However, detail of the damage is not known. We have already developed a method for estimating degree of localization of apurinic/apryrimidinic (AP) sites on DNA using Förster resonance energy transfer (FRET). The FRET efficiency ( $E$ ) was calculated using the donor fluorescence intensities before/after enzymatic digestion of the labeled AP-DNA [1]. Now we have tried to apply the method to  $^4\text{He}^{2+}$ - and  $^{60}\text{Co}$   $\gamma$ -irradiated DNA.

### EXPERIMENTS:

#### ● Sample preparation and He beam irradiation

Plasmid DNA digested by Sma I was used (linear formed). One hundred microliters of the DNA aq. (0.5 g/L) was transferred to an irradiation chamber (Fig.1), and was irradiated with linear energy transfer (LET) of  $\sim 70$  keV/ $\mu\text{m}$  of  $^4\text{He}^{2+}$  beam (TIARA, Japan Atomic Energy Agency), which was controlled by a depth-tunable cell irradiation equipment at r.t..  $^{60}\text{Co}$   $\gamma$ -rays (Kyoto University Research Reactor Institute: KURRI) were also used as a standard radiation source.

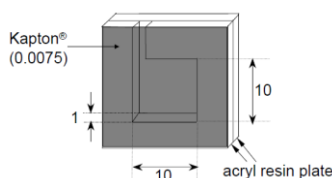


Fig.1. Irradiation chamber (mm)

#### ● Preparation of fluorophore-labeled irradiated DNA and the fluorescence spectroscopy for FRET observation

The irradiated DNA (10  $\mu\text{L}$  in water) and 10  $\mu\text{L}$  of 100 mM Tris-HCl (pH7.5) were mixed in a microtube. Two microliters of a mixture containing AF350 (donor fluorescent probe) and AF488 (acceptor one) with a given molar ratio was added to the DNA solution and was incubated for 24 h at 37°C. The fluorophore-labeled DNA was purified by ethanol precipitation. Twenty microliters of water was added to the residue. The fluorescence intensities were measured both at 449 nm (ex. 347 nm for AF350) and at 520 nm (ex. 460 nm for AF488). After the measurement, the enzyme cocktail containing DNase I

and phosphodiesterase I was added to the solution, and it was incubated for 2 h at 37°C.  $E$  values were calculated from the donor intensity before/after the digestion.

### RESULTS AND DISCUSSION:

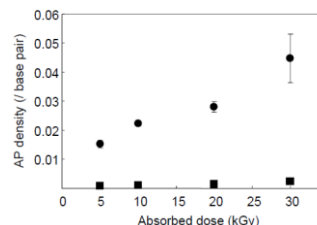


Fig.2. Relationship between absorbed dose and AP density for He ion beam (■) and  $^{60}\text{Co}$   $\gamma$ -rays (●).

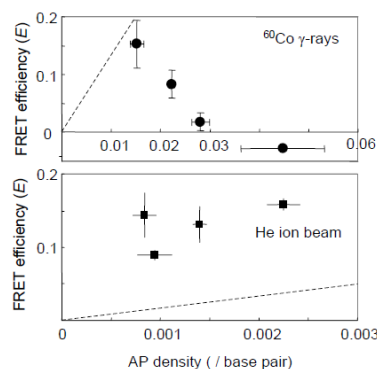


Fig.3. Relationship between AP density and FRET efficiency for He ion beam (■) and  $^{60}\text{Co}$   $\gamma$ -rays (●). The dashed lines indicate theoretical lines for randomly-distributed AP in DNA.

The He beam is stopped completely by DNA aq. (1 mm depth, see Fig.1), and all of the energy is transferred into the solution. It should be noted that the energy deposition may not be homogeneous although diffusion of DNA molecules can be promoted by vibration of the chamber during irradiation. Fig. 2 shows clear difference in the AP density (the number of AP sites produced/total DNA base pairs in the solution) between these radiation sources. Elimination of OH radicals by recombination would be responsible for the low level AP production for the high-LET He beam. In Fig.3, decrease of  $E$  for  $^{60}\text{Co}$   $\gamma$ -rays would be caused by gross fragmentation of DNA due to the numerous lesions. More data of lower dose region are needed. The  $E$  values for He beam are much higher than those for randomly-distributed AP. This seems that He beam produces clustered AP regions more frequently than random case. However, deeper consideration in heterogeneity of the energy deposition should be important for more proper estimation of the damage localization. Improvement of the irradiation system may also be needed.

### REFERENCE:

- [1] K. Akamatsu, N. Shikazono, *Anal. Biochem.* **433** (2013) 171-180.

H. Terato and T. Saito<sup>1</sup>*Analytical Research Center for Experimental Sciences, Saga University*<sup>1</sup>*Research Reactor Institute, Kyoto University*

**INTRODUCTION:** We have thought existence of a specific form of radiation damage, and are recently starting to consider clustered DNA damage (CDD) as one of the damage. CDD contains multiple lesions in the limited region of target DNA molecule caused by passage of radiation beam track. High-LET radiations such as heavy ion beams generate more condense and vast form of the track than low-LET radiation such as gamma-ray and X-rays. Thus, heavy ion beams are thought to produce larger number of CDD than low-LET radiations. In this regard, we indicated that yields of CDD decreased in elevation of the LET in the DNA molecule target irradiated *in vitro* (gamma > carbon > iron) [1]. We also reported that the isolated DNA damage showed similar trend for the LET's elevation. In this study, we simultaneously analyze the yields of DNA damage including CDD and surviving fractions of the irradiated cells to discuss the connection between the CDD and the impact of radio-biological effectiveness in heavy ion beam irradiation.

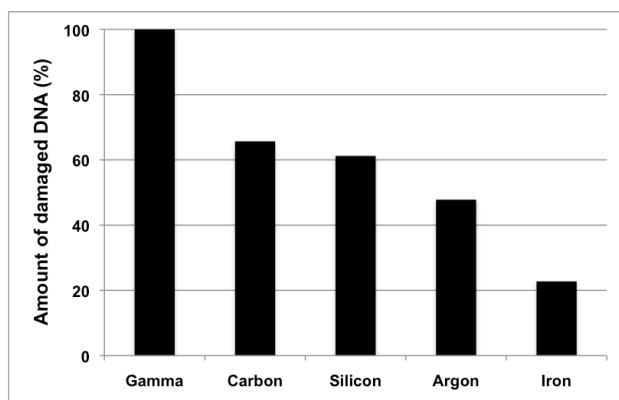
**EXPERIMENTS:** Chinese hamster ovary (CHO) A48 cells growing exponentially were irradiated by gamma-ray (0.2 keV/ $\mu\text{m}$ ), and carbon (13 keV/ $\mu\text{m}$ ), silicon (55 keV/ $\mu\text{m}$ ), argon (90 keV/ $\mu\text{m}$ ) and iron (200 keV/ $\mu\text{m}$ ) particle beams, respectively (parenthetic numbers indicate respective LETs). The gamma-irradiation was at <sup>60</sup>Co-gamma-source at KURRI, and those heavy ion beams were obtained from HIMAC at NIRS. The irradiated cells were embedded into agarose plugs, and

then the plugs were treated with endonuclease III and Fpg for CDD containing oxidative pyrimidine and purine lesions, respectively. Finally, the plugs were subjected to static field agarose gel electrophoresis (SFGE) to estimate CDD yields.

Also, we analyzed isolated DNA damage including oxidative base lesions by aldehyde reactive probe (ARP). The cultured cells were irradiated by those radiations, and the chromosomal DNA was extracted from the irradiated cells by NaI. The DNA were treated by the appropriate DNA glycosylases mentioned above, for identification of base lesions and then modified by ARP. Finally, we analyzed the ARP-modified DNA by ELISA-like procedure.

The radio-biological effectiveness of the irradiated cells was estimated by colony forming assay. The detail of analysis procedures was on our previous report [1].

**RESULTS:** SFGE analyses showed that the total CDD decreased in the elevation of the LETs (gamma > carbon > silicon > argon > iron) (Fig. 1). Similarly, the total isolated DNA damage decreased in elevation of the LETs (Fig. 2). These results conform our previous result of DNA solution [1]. On the other hand, colony forming assay showed that the radio-biological effectiveness corresponded to the LET-elevation (data not shown). The present result indicates that the relationship between yields of DNA damage including CDD and radio-biological effectiveness is imbalance. Thus, CDD seems to contribute the effect of heavy ion beams with its some characters other than the quantity. For instance, we must consider the importance of the quality, namely, the variation of constituent lesions and the distribution in a CDD for repair efficiency.

**REFERENCES:**[1] Terato H, *et al.*, J Radiat Res **49** (2008) 133-146.

**Fig. 1.** The yields of clustered DNA damage (CDD) in the irradiated cells.

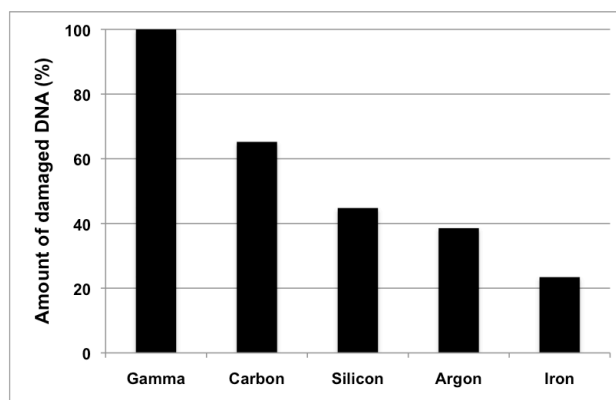


**Fig. 2.** The yields of isolated DNA damage in the irradiated cells.

## CO6-5 NAA for Trace Elements in Scalp Hair of Patients with ALS (the second report)

T. Kihira, I. Sakurai, S. Yoshida, I. Wakayama, K. Takamiya<sup>1</sup>, Y. Nakano<sup>1</sup>, R. Okumura<sup>1</sup>, Y. Iinuma<sup>1</sup>, K. Iwai<sup>2</sup>, K. Okamoto<sup>3</sup>, Y. Kokubo<sup>4</sup> and S. Kuzuhara<sup>4,5</sup>

Department of Health Sciences, Kansai University of Health Sciences (KUHS)

<sup>1</sup>Research Reactor Institute, Kyoto University

<sup>2</sup>Faculty of Nursing, KUHS

<sup>3</sup>Department of Public Health, Aichi Prefectural College of Nursing and Health

<sup>4</sup>Department of Neurology, Mie University Graduate School of Medicine

<sup>5</sup>Department of Medical Welfare, Suzuka University of Medical Science

**INTRODUCTION:** A high incidence of amyotrophic lateral sclerosis (ALS) has continued in the Koza / Kozagawa / Kushimoto (K) area in the Kii Peninsula of Japan. We previously reported an elevation of transitional metals in the scalp hair by NAA at KUR, and an elevation of urinary 8-hydroxydeoxyguanosine (8-OHdG), an oxidative stress marker, of patients with ALS in this area (K-ALS) [1]. Environment and lifestyle might play a role in increasing oxidative stress on patients with K-ALS. To examine the hypothesis that chronic Ca deficiency induce an increase of absorption of toxic metals, and consequently increase metal-induced oxidative stress on neurons, we compared metal contents in the scalp hair among patients with ALS in the K area, patients with sporadic ALS and residents in the Muro district.

**EXPERIMENTS:** Approximately 200 mg of hair was obtained from patients with K-ALS, patients with sporadic ALS, residents in the Muro district and controls. The hair samples were washed with 50 ml acetone, 50 ml d.d.w. (3 times) and 50 ml acetone in sequence. The samples were then dried in air. Approximately 30 mg of the sample was weighed and double-wrapped in polyethylene films and subjected to NAA. The samples in polyethylene capsules were irradiated in Pn-1 of KUR (1000 kW) for 2 minutes as short irradiations and for 120 minutes as long irradiations. As comparative standards, orchard leaves (NBS), a human hair standard (NIES, CRM No.13) and elemental standards were used. The  $\gamma$ -ray spectroscopic measurements with a Ge detector were performed repeatedly according to the protocol previously reported [2].

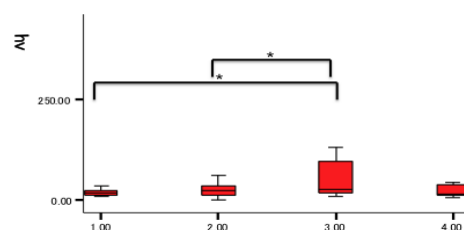


Fig 1. The V contents in hair samples were shown (ppb, boxes indicate median values, 25 and 75 percentiles). 1: controls, 2: residents in the K area, 3: patients with K-ALS, 4: patients with sporadic ALS (\*:  $p < 0.05$ ).

**RESULTS:** Hair samples from seven patients with K-ALS, 10 patients with sporadic ALS, 86 K-residents and 19 controls were collected between 2010 and 2012 and the contents of Ca, Al, Cu, Mn and V were analyzed. The samples were not treated with chemical procedures including perm. The contents of V ( $148.3 \pm 277.4$  ppb, mean  $\pm$  S.D.) and Mn ( $0.75 \pm 0.66$  ppm) of patients with K-ALS were higher than those of the controls ( $19.2 \pm 11.1$ ,  $0.22 \pm 0.35$ , respectively,  $p < 0.05$ , Fig. 1). Some of the K-residents showed high V in the hair; however, the mean content ( $28.6 \pm 27.9$  ppb) was not significantly different from the controls.

**DISCUSSION AND CONCLUSIONS:** The present results indicate that the contents of V and Mn in the scalp hair of patients with K-ALS were elevated. These transitional metals may play a role in increasing oxidative stress on patients with K-ALS.

Part of this report is submitted to 24<sup>th</sup> International Symposium on ALS/MND held at Milan, Dec. 2013.

### REFERENCES:

- [1] Kihira T, *et al.* Internal Medicine (2013), in press.
- [2] Kihira T, *et al.* KUR Report (2012).

## CO6-6 Mechanism Involved in Tumor Tissue of Colon 26 Carcinoma-Bearing Mice Irradiated with Neutron in the Presence of BSH-Appended Polyamine

T. Nagasaki, R. Kawasaki, M. Sakuramoto, H. Azuma, H. Yanagie<sup>1</sup>, Y. Hattori<sup>2</sup>, M. Kirihata<sup>2</sup>, K. Ono<sup>3</sup>, S. Masunaga<sup>3</sup> and Y. Sakurai<sup>3</sup>

Graduate School of Engineering, Osaka City University

<sup>1</sup>Graduate School of Engineering, The University of Tokyo

<sup>2</sup>Research Center for BNCT, Osaka Prefecture University

<sup>3</sup>Research Reactor Institute, Kyoto University

**INTRODUCTION:** Recently, we synthesized a novel polymeric boron carrier based on biodegradable polyamine,  $\epsilon$ -poly-L-lysine, followed by cross-linking and modified with the boron cluster, BSH (BPP, Fig. 1) [1]. Since this polymeric <sup>10</sup>B carrier has anionic zeta-potential, polyanion complexes with cationic polymer (nEG-PLL, Fig.1) afford nanoparticles suitable for safe and effective delivery into tumor tissues due to Enhanced Permeability and Retention (EPR) effect. The neutron-irradiation experiment was carried out with the complex in colon 26 carcinoma-bearing mice. Significant depression effect for the tumor proliferation was observed. Herein, mechanism of tumor growth suppression was assessed using well-characterized TUNEL assay.

**EXPERIMENTS:** Colon 26 cells ( $8 \times 10^5$  cells) were transplanted into a left thigh of mice (4 weeks old BALB/c, male). After 10 days of transplantation, BPP complex (BPP/23EG-PLL/9EG-PLL=8/4/1 w/w/w) solution was injected *via* tail vein at a dose of 4.0 mg <sup>10</sup>B/kg (400 ppm of <sup>10</sup>B concentration; 200  $\mu$ L). Twelve hours after injection, neutron irradiation ( $4 \times 10^{12}$  fluence/cm<sup>2</sup>) was carried out at Kyoto University Reactor (1 MW, 90 min). The mice were sacrificed 24 h and 48 h after neutron

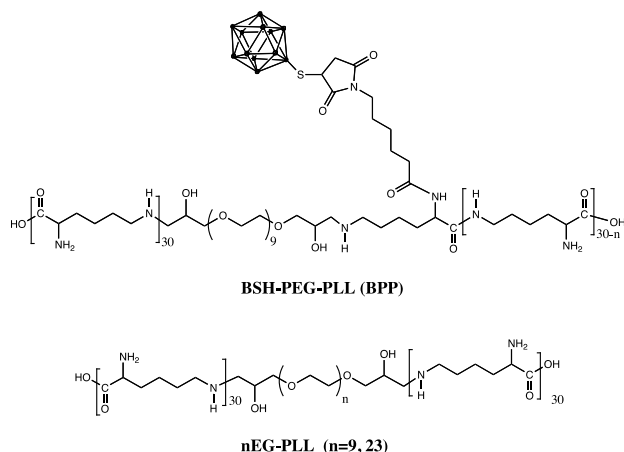


Fig. 1. BSH-appended polyamine and based polyamines.

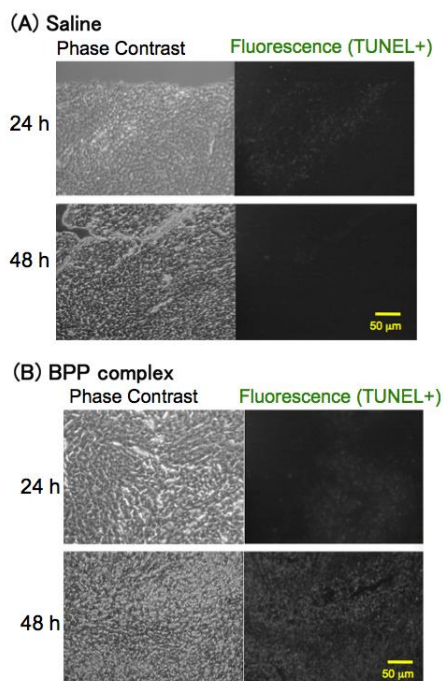


Fig. 2. TUNEL staining of tumors irradiated with neutron in the absence (A) and presence (B) of administrated BPP complex.

irradiation, and the tumor tissues were taken out and fixed by freezing with compound. Ten  $\mu$ m sections of tumor were stained with terminal deoxynucleotidyl transferase-mediated 'nick-end' labeling (TUNEL) using a In Situ Cell Death Detection Kit, Fluorescein (Roche).

**RESULTS AND DISCUSSION:** When tumor-bearing mice injected with BPP complex was irradiated with neutrons, significant depression effect for the tumor proliferation was observed (date not shown). Moreover, TUNEL staining of thin sections of tumor tissues after injection of BPP complex and neutron irradiation showed the DNA fragmentation (Fig. 2). After 48 h of irradiation highest DNA fragmentation was observed. These results indicated that BNCT with BSH-appended polyamine induced apoptosis of tumor cells *in vivo*.

### REFERENCE:

[1] M. Umamo *et al.*, Appl. Radiat. Isot., **69** (2011) 1765-1767.

採択課題番号 24022 ホウ素クラスター修飾ポリアミンの腫瘍集積性および  
中性子捕捉反応効率評価

共同通常

(阪市大院・工) 長崎 健、東 秀紀、李 家暉、鹿子嶋祐太、林高一郎、河崎 陸、櫻本昌士、  
湯川寛子 (東大院・工) 柳衛宏宣 (阪府大・BNCT 研) 切畑光統、服部能英、門野尚之  
(京大・原子炉) 小野公二、増永慎一郎、櫻井良憲

M. Okumura<sup>1,4</sup>, Y. Hidaka<sup>2</sup>, G. Inoue<sup>1</sup>, N. Fujii<sup>3</sup>, N. Fujii<sup>3</sup>, and H. Yamaguchi<sup>1</sup>

<sup>1</sup>*School of Science and Technology, Kwansei Gakuin University*

<sup>2</sup>*Graduate School of Science and Engineering, Kinki University*

<sup>3</sup>*Research Reactor Institute, Kyoto University*

<sup>4</sup>*Institute of Multidisciplinary Research for Advanced Materials, Tohoku University*

**INTRODUCTION:** The disulfide bond(s) play a critical role in the stabilities of their tertiary structures for the expression of biological activities. The disulfide bond formation thermodynamically and kinetically controls under redox conditions [1], for instance, concerning the role of glutathione, cysteine, protein disulfide isomerase (PDI), and PDI oxidase. These catalyze the formation, breakage, and isomerization of disulfide bond(s) *in vivo* or *in vitro*. Recently, we demonstrated that a positively charged redox reagent is preferred for accelerating disulfide-exchange reactions, as evidenced by the fact that the folding recovery is greater than that for a typical redox system [2,3,4]. Although the disulfide bond formation and the tertiary structure of a target protein are affected by redox molecules, the nature of the redox environment related to protein folding remains a matter of debate. The objective of this research is to elucidate the disulfide-coupled folding mechanism by *de novo* designed peptides as a redox molecule.

#### EXPERIMENTS:

**Peptide Synthesis-** The peptides were synthesized by the Fmoc solid-phase method using a PSSM-8 peptide synthesizer (Simadzu, Kyoto). The resulting peptides, containing several cysteine residues, were air-oxidized to form an intramolecular disulfide bond and the product was purified by RP-HPLC (Hitachi High-Technologies Corporation, Tokyo). The purified peptides were confirmed by MALDI-TOF/MS (Bruker Daltonics, Kanagawa) and stored in 0.1 M Tris/HCl buffer (pH 8.0) at room temperature until used.

**Preparation of reduced/denatured proteins-** The reduced/denatured proteins were prepared according to previously method [2], that is, purchased materials dissolved in 0.1 M Tris/HCl (pH 8.3) containing 20 mM dithiothreitol and 8 M urea, and the supernatant was allowed to stand for 3 h for room temperature. The mixture was then dialyzed against 10 mM HCl and lyophilized.

**Micrococcus luteus assay-** The refolding reaction was performed in 0.1 M Tris/HCl pH 8.0 buffer containing 1.0 mM GSH and 0.2 mM GSSG in the presence or absence of 1 mM synthesized peptide (peptide A or B). A *Micrococcus luteus* suspension (0.5 mg/mL) in 50 mM

phosphate buffer pH 6.5 was prepared to determine the bacteriolysis activity. The bacteriolysis reaction was started by mixing 10  $\mu$ L the refolded lysozyme solution and 1 mL a *Micrococcus luteus* suspension, and was quenched by adding a quenching solution containing 0.5 M iodoacetic acid, 1 M KOH, 1 M Tris/HCl buffer pH 7.0 [3,4]. The light scattering intensities of the reaction mixtures were measured at 600 nm.

**Oxidative folding analyses-** The denatured/reduced proteins were dissolved in 0.1 M Tris/HCl pH 8.0 in the presence of 2 mM reductant and 1 mM oxidant at room temperature for 48 hr, as described previously [2,3]. All solutions used in the folding experiments were flushed with N<sub>2</sub> gas. The reaction mixtures were removed at several time points, quenched with an equivalent volume of 1 M HCl [2,3], and separated by RP-HPLC. The HPLC fractions were analyzed by MALDI-TOF/MS.

**RESULTS:** To estimate the efficiency for coupled protein folding using the designed redox reagents, we employed to lysozyme, bovine pancreatic trypsin inhibitor (BPTI), and prouroguanylin as a model protein. In the case of lysozyme folding, peptide A or B accelerates the disulfide coupled protein folding as compared to a typical glutathione redox system, resulted in the increase of refolding yield.

By using HPLC analysis of disulfide-coupled folding of BPTI we found that synthesized peptide A or B accelerates the formation and the isomerization of intra-molecular disulfide bonds: the folding intermediates of BPTI were rapid rearrange to native form with correct disulfide bonds pairings as compared to a typical glutathione redox system.

In general, several disulfide-containing proteins such as lysozyme, BPTI, and RNaseA require redox condition to fold correctly *in vivo* or *in vitro*, because proteins in which cysteine residues are involved in folding are folded into the native conformation *via* the formation of agent-mixed disulfide intermediates under redox conditions. It is therefore a complicated problem to choice the folding condition with redox environment. This work demonstrated a redox molecule is preferred in accelerating the disulfide coupled folding and the new approach is effective in catalyzing the disulfide coupled protein folding. To elucidate the disulfide coupled protein folding mechanism further, folding experiments in detail using folding intermediates of prouroguanylin and BPTI are already in progress.

#### REFERENCES:

- [1] M. Okumura *et al.*, FEBS J., **279** (2012) 2283-2295.
- [2] M. Okumura *et al.*, FEBS J., **278** (2011) 1137-1114.
- [3] M. Okumura *et al.*, FEBS Lett, **586** (2012) 3926-3930.
- [4] L. Ito *et al.*, Protein J, **31** (2012) 499-530.

M. Fukushima, Y. Nakano<sup>1</sup>, R. Okumura<sup>1</sup> and  
A. Yoshihara

*Department of Basic Sciences, Ishinomaki Senshu  
University*

<sup>1</sup>*Research Reactor Institute, Kyoto University*

**INTRODUCTION:** In 2011 March 11, great earthquake and Tsunami attacked Pacific side of Main Island, Japan. Tsunami brought great amount of marine sediment to land, and after Tsunami we found the geographical feature of ocean floor has changed. In this study, we have analyzed multi-elements in marine samples including marine sediments, shellfishes, marine invertebrates by neutron activation analysis to compare them with elemental levels of samples obtained before The Great East Japan Earthquake.

**EXPERIMENTS:** <Samples> Marine sediment, oysters, mussels, and sea squirt were collected in two different points (Higashimatsushima and Makinohama in Oshika Peninsula) in Sendai Bay. Marine sediment was dried for 12 hours at 60 °C. Soft tissues of oysters were separated from shells, hepatopancreas, muscles, gills, and mantles were separated each other, and freeze dried. Dried samples were pulverized by mill. Soft tissues of mussels were separated from shells, freeze dried, and pulverized by mill. Sea squirt was washed with tap water, freeze dried, and pulverized by mill. <Neutron Activation Analysis> 0.3-0.5 g of dried samples were heat sealed doubly by cleaned polyethylene seat, and irradiated with several kinds of Standard Reference Materials (SRM). Irradiation was done for 12 seconds by Tc-Pn or Pn, 1 minute by Tc-Pn, 20 minutes by Pn, and 4 hours by Pn. After appropriate cooling time, gamma rays of irradiated samples were measured by Ge detector. For 12 second irradiation, Compton suppression system (CSS) was used for measuring. Elemental levels were calculated from the specific sensitivity of SRM.

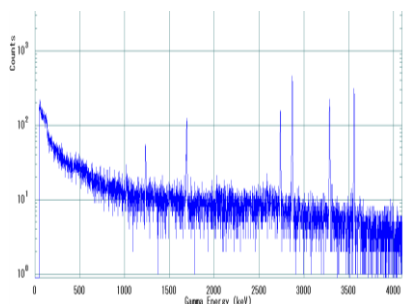


Fig. 1 Gamma spectrum of sea squirt by CSS after 12 second irradiation.

**RESULTS:** Typical gamma spectrum by CSS is shown in Fig. 1, and gamma spectrum by normal Ge detector is shown in Fig. 2. By using CSS, it is obvious the back ground level for lower energy range has lowered. Elemental levels are shown in Table 1 for several samples for the example without error. We have analyzed several elements in hepatopancreas of oysters from same collection point before The Great East Japan Earthquake. The levels were 0.15, 198, 0.13, 0.03, and 477 ppm (dry weight base) for Co, Fe, Rb, Sc, and Zn, respectively. By comparing them each other, we can say that Fe level changed lower and Rb level changed higher, and other elemental levels did not change. We will continue the analysis of these samples for further work.

Table 1. Elemental levels of samples obtained by NAA ( $\mu$  g/g, dry weight).

Element	marine sediment	Sea squirt ( <i>Ciona savignyi</i> )	oyster, hepatopancreas
Al	19000	12300	ND
Br	64	226	188
Co	8.55	2.56	0.23
Cs	2.6	0.76	0.03
Fe	31700	6720	94.4
Mn	237	157	ND
Rb	45.1	12.2	3.8
Sc	5.5	32	0.02
Zn	93.7	77.2	488

**Acknowledgement:**

We thank to Mr. Shigeru Watanabe and his family, Dr. Takeshige Matsutani in Ishinomaki Senshu University for their help for collecting samples.

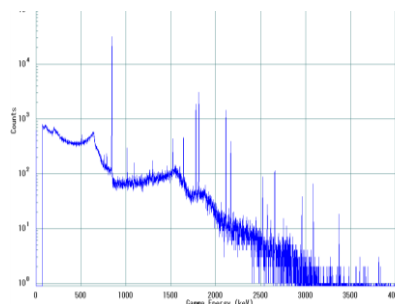


Fig. 2 Gamma spectrum of sea squirt by normal Ge detector system after 12 second irradiation.

## CO6-9 Evaluation of Time-Dependence of the Concentration of Gadolinium-Based Contrast Agent, Manganese, and Zinc in Normal and Nephrectomized Mice

K. Washiyama, T. Matsumoto, E. Shinohara, Y. Nakaniishi, Y. Murasaki, R. Amano and K. Takamiya<sup>1</sup>

School of Health Sciences, College of Medical, Pharmaceutical and Health Sciences, Kanazawa University

<sup>1</sup>Research Reactor Institute, Kyoto University

**INTRODUCTION:** Gadolinium (Gd)-based contrast agents (GBCAs) have been used in medical magnetic resonance (MR) imaging. In particular, human nephrogenic systemic fibrosis (NSF) has been reported in patients with severe renal insufficiency treated with Gd-based contrast agent [1]. A depletion of endogenous Zn ion is proposed as one of the reasons for development of NSF [2, 3]. On the other hand, there also reported no correlation between Zn and NSF [4]. Our recent findings also showed no correlation of Zn with both GBCA and nephrectomized situations [5]. However, those results were obtained from only one time point after GBCA administration (2 days) and, therefore, the relation between Gd and trace elements *in vivo* is still unclear.

In this study, we evaluated the time dependence of both the distribution of Gd and concentration of some minerals by neutron activation analysis (NAA) in selected tissues of four mice under different experimental conditions.

**EXPERIMENTS:** Forty-one male 8-week-old ICR strain mice were used in this study. Twenty-four mice were housed as normal, while another seventeen mice were partially nephrectomized as pseudo renal impairment model [6]. Half of each group was administered 2.5 mmol Gd/kg b.w. Omniscan (gadodiamide) intravenously. Mice were sacrificed and dissected 1, 3, 7 days after administration according to the experimental conditions. Blood samples were collected, and the femur, kidney, and liver were excised and weighed. The samples were freeze-dried and sealed into polyethylene bags for NAA. The sealed samples and standard of gadolinium were irradiated in Pn-3 for 30 s and in Pn-2 for 1 h, for short and long half-life radioisotopes production, respectively. The distribution of Gd and concentration of minerals were determined by  $\gamma$ -ray spectrometry.

**RESULTS AND DISCUSSION:** Almost of all the selected tissues in nephrectomized (model) mice showed high Gd concentration compared to normal mice during the experimental period. Gd concentration decreased with time except for the femur in model mice, in which Gd increased for 7 days (Fig.1). Due to the bone seeking property of Gd and the low rate of the renal metabolism compared to normal mice, Gd seems to accumulate in the femur in the model mice at a higher concentration.

The concentration of Mn in the liver and Zn in the skin are shown in Fig. 2. The liver of Gd-administered model mice showed increased Mn concentrations compared to normal mice. Zn concentration in model mice was high compared to other groups after 1 day of Gd administration. On the other hand, Gd-administered model mice showed high Zn concentration after 7 days.

We evaluated the time-dependence of the concentration of “exogenous” Gd and “endogenous” Mn and Zn. However, these results do not sufficiently provide statistically warranted representations of the biodistribution of “exogenous” Gd and the concentration of “endogenous” and “exogenous” trace elements in normal and model mice to clarify the correlation between Gd and trace elements.

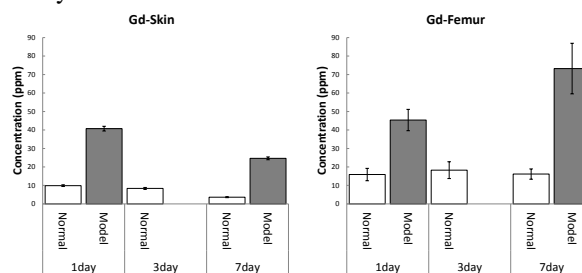


Fig. 1. Time dependence of the concentration of Gd in the skin and femur of normal and nephrectomized mice after GBCA administration. White and gray bars represent normal mice and nephrectomized mice, respectively.

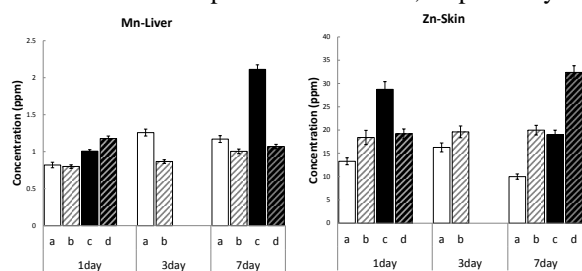


Fig. 2. Time dependence of the concentration of Mn in the liver and Zn in the skin of normal and nephrectomized mice after GBCA administration. White, black, and striped bars represent normal mice, model mice, and groups of GBCA administration, respectively.

### REFERENCES:

- [1] J. C. Weinreb and A. K. Abu-Alfa, *J. Magn. Reson. Imaging*, **30** (2009) 1236-1239.
- [2] E. S. Harpur *et al.*, *Invest. Radiol.*, **28** (Suppl 1) (1993) S28-S43.
- [3] J. H. Wible *et al.*, *Invest. Radiol.*, **36** (2001) 401-412.
- [4] H. Pietsch *et al.*, *J. Magn. Reson. Imaging*, **30** (2009) 374-383.
- [5] K. Washiyama *et al.*, *KURRI Progress Report 2011*, (2012) PR1-6.
- [6] H. Pietsch *et al.*, *Invest. Radiol.*, **44** (2009) 226-233.

採択課題番号 24080 MRI用ガドリニウム造影剤による副作用「腎性全身性線維症」 共同通常の発症機序の解明に関する研究

-アクチバブルトレーサー法の応用- (原子炉中性子を用いた微量元素分析)

(金沢大・保健) 鷺山幸信、松本高史、篠原絵里香、中西勇介、村崎祐一、天野良平  
(京大・原子炉) 高宮幸一

# CO6-10 Mössbauer Studies on Reversible O-O Bond Scission of Peroxodiiron(III) to High-Spin Oxodiiron (IV)

M. Kodera, Y. Kawahara and S. Kitao<sup>1</sup>

Department of Molecular Chemistry and Biochemistry,  
Doshisha University

<sup>1</sup>Research Reactor Institute, Kyoto University

**INTRODUCTION:** Soluble methane monooxygenases (sMMO) are non-heme diiron enzymes catalyzing conversion of CH<sub>4</sub> to CH<sub>3</sub>OH, one of the most difficult chemical oxidation, via a dioxygen activation, where intermediate P, peroxodiiron(III) generated by O<sub>2</sub>-binding to diiron(II), is converted to active species Q, oxodiiron(IV) responsible for the CH<sub>4</sub> oxidation[1-3]. The diiron(IV) of Q is in a high-spin S = 2 state.<sup>3</sup> A di- $\mu$ -oxodiiron(IV) diamond core structure is proposed for Q from the short Fe••Fe distance (2.5 Å),[4] but not established. The conversion of P to Q, however, has not been clarified due to their instability [3,5] Thus, a functional model attaining conversion of peroxodiiron(III) to high spin oxodiiron(IV) is useful for clarification of the P-to-Q conversion mechanism.

Recently, we succeeded in spectral observation of the reversible O-O bond scission of peroxodiiron(III) to oxodiiron(IV) with a bis-tpa dinucleating ligand 6-hpa (1,2-bis[2-bis(2-pyridylmethyl)aminomethyl]-6-pyrid-yl]ethane)[6].

We report herein the Mössbauer measurements of the conversion of the peroxodiiron(III) to the oxodiiron(IV).

**EXPERIMENTS: Preparation of a mixture of peroxodiiron(III) and oxodiiron(IV) complexes 2.** To a solution of [Fe<sub>2</sub>( $\mu$ -O)(OH)<sub>2</sub>(6-hpa)](ClO<sub>4</sub>)<sub>4</sub> (**1**) (45.1 mg 36.3  $\mu$ mol) in MeCN (2.5 mL) was added 2.0 equiv of Et<sub>3</sub>N (29 mM) at -40°C, and stirred for 5 min. To the solution was added 1.2 equiv of H<sub>2</sub>O<sub>2</sub> (17 mM), and stirred for 2 min. The solution turned dark green. To the resultant solution was added 20 mL of Et<sub>2</sub>O at -40°C, green solid precipitated. The supernatant was decanted off, and the precipitate was washed with Et<sub>2</sub>O several times at -40 °C. The green solid was dried in vacuo. The isolated solid is stable at low temperature, and not changed several days at room temperature under dark in the absence of any organic compounds potentially acting as reductant. Yield 31.3 mg (33.8  $\mu$ mol, 93.1 %). Anal. Calcd for C<sub>38</sub>H<sub>46</sub>N<sub>8</sub>Cl<sub>2</sub>O<sub>15</sub>Fe<sub>2</sub>: C, 43.99; H, 4.47; N, 10.80%. Found: C, 44.21; H, 4.32; N, 10.69%. The isolated solid was used for various spectral measurements including the Mössbauer spectra.

**RESULTS:** In the previous studies, the Mössbauer spectra of the isolated solid **2** were recorded between 25 and 295 K at zero field. The spectrum at 25 K is composed of two quadrupole doublets with  $\delta = 0.351(3)$  mm/s,  $\Delta E_Q = 1.635(5)$  mm/s and  $\delta = 0.132(9)$ ,  $\Delta E_Q = 0.438(2)$ , as shown by the deconvolution spectra, the red and blue lines in Figure 1(a), respectively. The  $\delta$  and  $\Delta E_Q$  values of the red line are close to 0.54 and 1.68 mm/s of  $\mu$ -oxo- $\mu$ -peroxodiiron(III) **5**, 0.66 and 1.40 mm/s of  $\mu$ -peroxo-di- $\mu$ -benzoato-diiron(III) with sterically hindered trispyrazolylborate HB(pz<sup>-</sup>)<sub>3</sub>, and 0.53 and 1.68 mm/s of  $\mu$ -peroxo-di- $\mu$ -acetato-diiron(III) of hexpy ligand. Thus, the red line may result from a diiron(III) symmetrically bridged

by the peroxide. The  $\delta$  and  $\Delta E_Q$  values of the blue line are close to  $\delta = 0.14$ - $0.21$  and  $\Delta E_Q = 0.53$ - $0.68$  mm/s of high spin S = 2 diiron(IV) in the active species Q of sMMO. The high spin S = 2 iron(IV) complexes reported so far show the  $\delta$  and  $\Delta E_Q$  values around 0.1 and 0.5 mm/s, respectively, but low spin S = 1 iron(IV) relatively higher  $\Delta E_Q$  values 1-2 mm/s. Thus, the blue line must be due to a high spin S = 2 diiron(IV) with a symmetric structure. These results and all other spectral and analytical data shown above demonstrated that **2** is composed of the  $\mu$ -oxo- $\mu$ -peroxodiiron(III) complex **2a** and the high spin S = 2  $\mu$ -oxo-dioxodiiron(IV) complex **2b**. Here, **2b** is the first synthetic example of a high-spin S = 2 oxodiiron(IV).

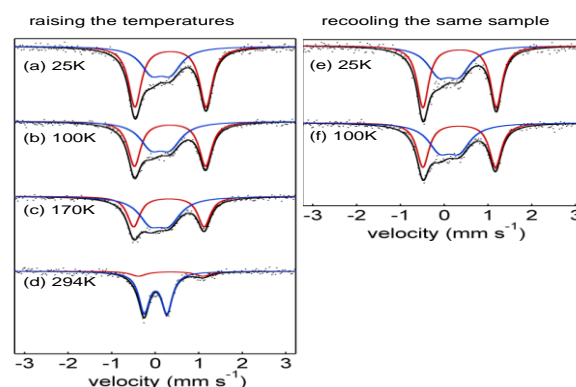


**Fig 1.** Zero field Mössbauer spectra of **2**, recorded by raising the temperature at (a) 25, (b) 100, (c) 170, and (d) 294 K, and by recoiling the same sample at (e) 25 and (f) 100 K. The black line is the least-square fitting to the raw data, and the red and blue lines are the deconvolution spectra corresponding to  $\mu$ -oxo- $\mu$ -peroxodiiron(III) (**2a**) and  $\mu$ -oxo-dioxodiiron(IV) (**2b**) complexes.

In this study, further, we tried to measure the Mössbauer spectra under applied magnetic field conditions. However, it was not successful because upon preparation of the KBr disk of the measurement sample, the peroxodiiron(III) complex was decomposed to a structurally unknown diiron(III) complex. So, we may need to improve the sampling method. In this year, we will try to optimize the sampling method and carry out some more experiments of the Mössbauer measurements under the applied magnetic field.

## REFERENCES:

- [1] Tinberg, C. E.; Lippard, S. J. *Acc. Chem. Res.* 2011, **44**, 280-288.
- [2] Friedle, S.; Reisner, E.; Lippard, S. J. *Chem. Soc. Rev.* 2010, **39**, 2768-2779.
- [3] Wallar, B. J.; Lipscomb, J. D. *Chem. Rev.* 1996, **96**, 2625-2658.
- [4] Shu, L.; Nesheim, J. C.; Kauffmann, K.; Münck, E.; Lipscomb, J. D.; Que, L. *Science* 1997, **275**, 515-518.
- [5] Liu, K. E.; Valentine, A. M.; Wang, D.; Huynh, B. H.; Edmondson, D. E.; Salifoglou, A.; Lippard, S. J. *J. Am. Chem. Soc.* 1995, **117**, 10174-10185.
- [6] M. Kodera, Y. Kawahara, Y. Hitomi, T. Nomura, T. Ogura, Y. Kobayashi, *J. Am. Chem. Soc.*, 2012, **134**, 13236.

## CO6-11 Determination of Trace Elements in Organs and Tissues of Zn-Deficient Mice

M. Yanaga, A. Oishi, K. Sera<sup>1</sup>, R. Okumura<sup>2</sup> and Y. Inuma<sup>2</sup>

Graduate School of Science, Shizuoka University

<sup>1</sup>Cyclotron Research Center, Iwate Medical University

<sup>2</sup>Research Reactor Institute, Kyoto University

**INTRODUCTION:** Previously, we reported that the Co content increased significantly in all the organs and tissues of Zn-deficient mice, which had been fed with Zn-deficient diet for 1 week, 3 weeks, or further period from 3 or 8-week old, compared with those of mice fed with control diet, and that this fact suggested the partial substitution of Co with Zn in their metal proteins or other metal-bound compounds.[1-3] In the present work, concentrations of trace elements in organs and tissues of mice were determined in order to examine whether cobalt functions as a substitute for zinc.

### EXPERIMENTS:

**Animals and preparation of samples** Male mice of the ICR/jcl strain, 8-week old, were divided into two groups. One group was fed with Co-enriched Zn-deficient diet (the diet was made with raw materials for Zn-deficient diet and Co as  $\text{CoCl}_2$ ) and ultra pure water (Co-enriched Zn-def. mice) for one or three weeks. The other one group was fed with Cu-enriched Zn-deficient diet (the diet was made with Cu as  $\text{CuSO}_4 \cdot 5\text{H}_2\text{O}$ ) and the same water (Cu-enriched Zn-def. mice).

After the treatment, about 1 mL of blood was collected from heart under diethyl ether anesthesia, and then, 5 organs and tissues such as liver, kidney, pancreas, testis, and bone were removed. The blood samples were centrifuged and the serum was harvested for PIXE analysis. The removed organs and tissues were weighed, freeze-dried, weighed again and grounded. Each sample was doubly wrapped in polyethylene film for INAA (Instrumental Neutron Activation Analysis).

**PIXE Analysis** One hundred  $\mu\text{L}$  of the serum was dropped on a backing film (polypropylene) and directly irradiated with proton beam at Nishina Memorial Cyclotron Center, Japan Radioisotope Association. The spectra were analyzed with the standard-free method. [4, 5]

**INAA** The samples in polyethylene capsules were irradiated in Pn-1 for 90 seconds and for 2 hours, for

short and long irradiation, respectively. The  $\gamma$ -ray spectroscopic measurements with an HPGe detector were performed repeatedly for the short-irradiated samples: the first measurements for 120 seconds after decay time of 5 - 10 minutes and the second one for 250 seconds after 80 - 120 minutes. The long-irradiated samples were measured for 3 - 24 hours after an adequate cooling time (60 - 80 days).

**RESULTS:** As results of PIXE analysis of the serum samples, Co concentration of Co-enriched Zn-def. mice was much risen whereas Cu concentration of Cu-enriched Zn-def. mice was not higher than that of Co-enriched Zn-def. mice. Similar trend was found for all the organs and tissues investigated by INAA. On the other hand, Zn concentration in pancreases of mice which were fed with Co-enriched Zn-deficient diet for three weeks was slightly restored as shown in Fig. 1. This might indicate that some kinds of mechanisms which enhance the intake of Co in all the organs and tissues of Zn-def. mice could be operated, and that Co would function to disturb that Zn flowed out.

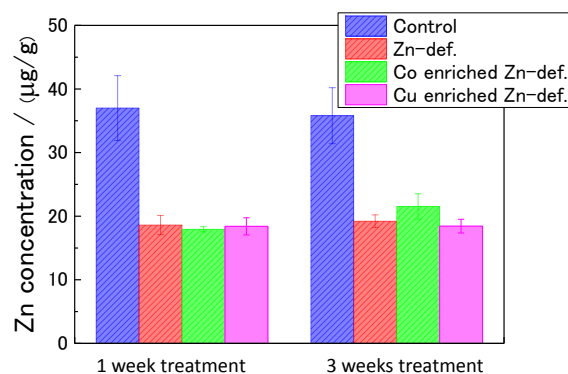


Fig. 1 Zn concentration in pancreases of mice

### REFERENCES:

- [1] M. Yanaga, M. Iwama, K. Takiguchi, M. Noguchi and T. Omori, *J. Radioanal. Nucl. Chem.*, **231** (1998) 187-189.
- [2] M. Yanaga, M. Iwama, K. Shinotsuka, K. Takiguchi, M. Noguchi and T. Omori, *J. Radioanal. Nucl. Chem.*, **243** (2000) 661-667.
- [3] M. Yanaga, H. Wakasa, T. Yoshida, M. Iwama, K. Shinotsuka, M. Noguchi and T. Omori, *J. Radioanal. Nucl. Chem.*, **245** (2000) 255-259.
- [4] K. Sera, S. Futatsugawa, K. Matsuda and Y. Miura, *Int'l Journal of PIXE*, **6**(1996) 467-481.
- [5] K. Sera, S. Futatsugawa, S. Hatakeyama, Y. Saitoh and K. Matsuda, *Int'l Journal of PIXE*, **7**(1996) 157-170.